Fabrication of Surface Embedded Silver Cellulose-based Flexible Transparent Electrodes by Self-Assembly

Wentao Zhang, Tianhao Wang, Ying Zhu, Yanan Gao, Lin Liu, Mengling Li, and Liping Zhang *

Developing eco-friendly, degradable, and flexible electronic devices using renewable cellulose, such as waste agricultural straw, is increasingly vital. This approach tackles the growing issue of nondegradable electronic waste. In this study, flexible transparent electrodes (FTEs) were created using cellulose from waste corn straw, embedding silver nanowires (AgNWs) networks within the surface layer. This method is suitable for reel-to-reel processing. These sustainable FTEs had high transparency and conductivity, with a film resistance of 45.4 Ω/sq and light transmittance of 86.2% at 550 nm. The "dissolution–regeneration" self-assembly process harnesses cellulose's hydrogen bond network to stabilize the AgNWs network, providing the FTEs with excellent electromechanical stability. Resistance changes were less than 3% during bending, folding, and 1,000-time cyclic bending tests. Furthermore, these electrodes showed remarkable environmental stability, with only a 2.5% resistance increase after 16 days at room temperature. This research demonstrates a new application for agricultural straw cellulose in flexible electronics, offering a sustainable alternative in electronic materials.

INTRODUCTION

The fields of photoelectric communication and energy conversion have experienced unprecedented growth (Hu *et al*. 2021). Flexible transparent electrodes (FTE) are general platforms for electric signal input and output channels and are widely used in solar cells (Fan 2021), flexible displays (Zhu *et al*. 2020), organic light-emitting diodes (Sun *et al*. 2022b), and transparent heaters (Li *et al*. 2020). However, their wide adoption in commercial and industrial applications may lead to a rise in non-degradable conductive plastics and plastic-based electronic materials, increasing the stress on the environment (Hamd *et al*. 2022). Biomass-based materials are alternatives to plastics and are expected to provide significant economic and environmental benefits (Janaswamy *et al*. 2022).

Corn straw cellulose is a biomass resource with very large reserves and underutilization (Gill *et al*. 2021). It is rich in hydroxyl groups, which can be modified easily with organic and inorganic units to form functional materials with desired properties (Aziz *et al*. 2023). Forming a conductive layer on its surface may be an effective strategy for the design of novel photoelectric devices (Min *et al*. 2012).

Despite the significant potential of highly conductive materials such as graphene in various fields as two-dimensional materials (Ashok Kumar *et al.* 2022), their large-scale

application faces challenges in preparation, transfer, and high costs (Shen *et al*. 2021). Particularly in flexible devices, the irregular shapes and grain boundary barriers of graphene nanosheets hinder the achievement of long-range electrical properties. (Qian *et al*. 2022). Addressing these challenges, developing new materials that are economical, simple to process, and highly conductive is crucial. The present research highlights the potential of silver nanowires (AgNWs) embedded in a cellulose matrix, forming a random network as flexible transparent conductors. This novel material offers an effective solution to overcome the limitations of existing materials. (Ma *et al*. 2021).

Recent reports on cellulose-based flexible electrode materials have focused on FTE films assembled by the preparation and filtration of nanocellulose and conductive materials (Zhang *et al*. 2019), but low transparency and high surface roughness limit their development (Sun *et al*. 2022a). Another potential technique involves ionic liquids, which are solvents with low boiling points (Valderrama *et al*. 2007) and high solubility (Rieland and Love 2020). Ionic liquids also can dissolve cellulose and regenerate the material in various forms (Xie *et al*. 2022). Regenerated cellulose films prepared by ionic liquids generally have high optical transmittance and low surface roughness (Guo *et al*. 2021), but there are only a few reports on flexible electrodes using regenerated cellulose.

To develop practical optoelectronic devices, it is important to scale up the size without compromising quality and performance (Qin *et al*. 2022). Cost-effective manufacturing of FTEs over large areas with high throughput is challenging, and much of the current effort is focused on spin coating (Wang *et al*. 2019) and spraying (Akter and Kim 2012) of low-cost precursors. Although this is an attractive solution for fabricating large samples, there are many problems. For example, with inkjet printing and spin coating processes, AgNWs with high aspect ratios are prone to agglomeration (Tan *et al*. 2021; Wu *et al*. 2021; Fan *et al*. 2022). The larger aspect ratios are desirable for simultaneously increasing light transmittance and electrical conductivity (Sang *et al*. 2022).

This research showcases the development of cellulose-based Flexible Transparent Electrodes (FTEs) composed of a randomly distributed network of silver nanowires (AgNWs) integrated into a cellulose surface layer. Utilizing a novel all-cellulose membrane material, characterized by its exceptional oxygen resistance, high light transmittance, and minimal surface roughness, this study successfully embeds AgNWs within a diluted cellulose solution. This creates a conductive network on the all-cellulose nanocomposite (ACNC) membrane's surface through an innovative "self-assembly strategy of dissolution and regeneration." The resulting cellulose-based FTEs exhibit a uniformly smooth surface along with remarkable photoelectric stability, making them highly suitable for thin film optoelectronic device production. One of the key strengths of this method is its compatibility with straightforward roll-to-roll processing, paving the way for scalable FTE manufacturing. The molecular self-assembly process not only ensures a low surface roughness but it also forms a stable and dense conductive layer, maintaining electronic performance even under deformation. Additionally, these films demonstrate considerable environmental durability. Compared to plastic substrates, the cellulose base offers numerous benefits, including abundant availability, renewability (Li *et al.* 2019), biodegradability (Zhao *et al.* 2019; Zhang *et al.* 2019), superior thermal stability, and a significantly lower thermal expansion coefficient (Calvino *et al.* 2020). Although the potential anaerobic decomposition of cellulose, leading to methane emissions, and the non-degradability of minute silver nanowires remain challenges, this study still presents a sustainable and cost-effective method for producing cellulose-based Flexible Transparent Electrodes (FTEs). It offers new perspectives and theoretical groundwork for broadening the application of functional fiber-based materials.

EXPERIMENTAL

Materials

Corn straw pulp with 84% cellulose and 2.34% lignin content was obtained from Jilin Chemical Fiber (Jilin, China). The degree of polymerization of the corn pulp was estimated to be 1700 to 1750 by measuring the solution of copper ethylenediamine hydroxide using an Ubbelohde viscometer (Shanghai Qihang Glassware Factory, China). All chemicals, including dimethyl sulfoxide (DMSO), polyvinyl pyrrolidone (PVP, M_w = 1,300,000), sodium chloride ($\geq$ 99.5%), glycerol (GL$\geq$ 99.0%), ethylene glycol (EG$\geq$ 99.0%), ethanol ($\geq$ 99.0%), sodium hydroxide, silver nitrate (AgNO$_3$, $\geq$ 99.8%), and ethylenediamine, were analytical grade and used without further purification (Beijing Chemical Works, Beijing, China). Deionized (DI) water was prepared using a laboratory water purification system.

Synthesis of AgNWs

AgNWs with an average diameter of 40 nm were synthesized using the conventional polyol method (Kumar *et al*. 2013). Briefly, a 200 mL flask containing 90 mL of ethylene glycol (EG) was heated at 160 °C for 20 min. Then, 0.031 mL of KBr solution was added. Next, 100 mL of 0.04M AgNO$_3$ solution and 100 mL of 0.66M PVP EG solution were injected into the flask and continued to react for 1 h. The obtained AgNWs were washed with ethanol and water and separated by centrifugation at 2500 rpm for 5 min, repeating the washing and centrifugation steps 3 times. Finally, the AgNWs were redistributed into DMSO.

Synthesis of ACNC

Ionic liquid solvent systems have been adopted in previous studies (Zhang *et al*. 2020), and a similar method was used with some modifications. Briefly, 3 g of dry cellulose material (For detailed information on the specific components used, please refer to the supplementary materials provided.) and 50 g of ionic liquid were placed in a 100 mL flask. A uniform cellulose suspension was obtained by heating the flask in an oil bath at 50 °C and stirring the material at 300 rpm for 6 h. A DMSO suspension cellulose nanofibers was uniformly mixed with the obtained cellulose solution at 0 to 4 °C. Next, the mixed liquid was poured onto a clean glass plate, and the film thickness was adjusted to 120 μm using an automatic film scraper. The film was left for 30 seconds after scraping and then soaked in DI water to remove the ionic liquid. Finally, the cellulose film was dried in an oven at 55 °C for 4 h to obtain a transparent ACNC film.

Fabrication of AgNWs/CE@ACNC Films

Figure 2 illustrates the steps used for forming films of AgNWs/CE@ACNC. First, the DMSO dispersion of AgNWs was added into the diluted cellulose solution with varying the mass ratios of AgNWs and cellulose solution (*i.e*., 5:1, 3:1, and 1:1) and stirred. The cellulose solution dispersed with AgNWs was evenly coated on the ACNC film moistened with DMSO by scraping, and then the entire film was placed in water for 5 min to induce solidification and regeneration. The finished hydrogel was immediately dried in an oven at 50 °C for 4 h. According to the mass ratio of AgNWs to cellulose ("CE"), the obtained samples were labeled as either AgNWs5/CE1@ACNC, AgNWs3/CE1@ACNC, or AgNWs1/CE1@ACNC.

Characterization of AgNWs/CE@ACNC Films

Scanning electron microscopy (SEM) and energy dispersive X-ray spectroscopy (EDS) were performed using an S-3400N microscope (Hitachi, Tokyo, Japan). The cellulose-based FTEs were dried at room temperature and sputtered with gold prior to observation using a sputter coater (SBC-12, Cressington, Watford, UK).

Transmissivity measurements were conducted using a UV-Vis spectrometer (PerkinElmer Lambda 650, Waltham, MA, USA) in the 400 to 900 nm range.

Atomic force microscopy (AFM) images were obtained using a Bruker Dimension Icon microscope with the FTE samples fixed on a glass plate. The surface roughness was studied using a scanning area of 5 μm × 5 μm.

The two ends of the dry samples (The strips of material measure roughly 14 cm in length and 1 cm in width.) were fixed in a tensile testing machine (Instron 5848, Norwood, MA, USA) to measure the tensile strength and elongation of the samples at failure.

The thermal properties of the membranes were characterized using a thermogravimetric analyzer (TGA550, TA Instruments, USA). Measurements were recorded under a nitrogen atmosphere with a heating rate of 10 °C/min, ranging from room temperature to 450 °C.

The structure of the films was analyzed by X-ray diffraction (XRD) using an XRD-6000 diffractometer (Shimadzu, Kyoto, Japan). Before measurement, the sample was vacuum-dried for 24 h. Spectra were acquired using CuK alpha radiation ($\lambda = 0.15418$ nm) at 40 kV and 40 mA with a scan rate of 2°/min over a 2θ range of 10° to 80°.

Oxygen transmission rates of the films were determined at 23 °C and 0% relative humidity (RH) using a permeability analyzer (C203H, Labthink, Boston, USA) under standard conditions (ASTM 3985). Each measurement was continued until the O_2 transmission rate reached a stable value. The oxygen permeability was determined from the oxygen transmission rate and the film thickness, and the standard deviations for each film were within ±5%.

An electric four-probe tester (ST-2258C, Jingge Electronic, Suzhou, China) was used to measure the sheet resistance of 10-cm × 10-cm films. The mean values are reported in this paper. The mechanical and electrical stability of the sample was evaluated by performing bending tests. The films were bent along the length direction until the two ends made contact, and the sheet resistance was measured several times every 100 bending cycles, for a total of 1000 bending cycles. To test the environmental stability of the surface square resistance, the films were exposed to air, and the sheet resistance was measured 10 times every 2 days.

A 6-cm × 1-cm AgNWs3/CE@ACNC sample was prepared for the light-emitting diode (LED) lamp test. In the test, two 1.5 V dry batteries and 3 mm LED lamp beads were connected in series with the bent sample.

In addition, the change in resistance during bending was also monitored using a multimeter. The multimeter was connected to both ends of the sample, as shown in Fig. 5(c), and the real-time resistance value was recorded as R_x. The resistance value of the sample in the flat and straightened state was recorded as R_0, and thus the change in resistance is $\triangle R = R_x - R_0$.

RESULTS AND DISCUSSION

Characterization of FTEs

The morphology of AgNWs is shown in Fig. 1(a). The length and width of the AgNWs in the SEM images were between 15 to 25 µm and 35 to 50 nm (Kumar *et al*. 2013), respectively. Additionally, almost no silver nanoparticles were present in the films. This was verified in the XRD pattern of the AgNWs, as shown in Fig. 2(d). The diffraction peaks at $2\theta = 38.24°$, $44.42°$, $64.54°$, and $77.46°$ correspond to the (111), (200), (220), and (311) crystal faces of silver (Gorji *et al*. 2021), respectively. No other impurity peaks were observed, indicating that the synthesized AgNWs consisted only of surface cubic phases and were of high purity. The peak shape was sharp, and the half-width was narrow, which indicates that the obtained AgNWs also had high crystallinity. In addition, the diffraction peak intensity of the (111) crystal plane was much higher than that of the other three crystal faces, indicating that the material grows predominantly in this direction, which is favorable for a high aspect ratio (Zhang *et al*. 2020).
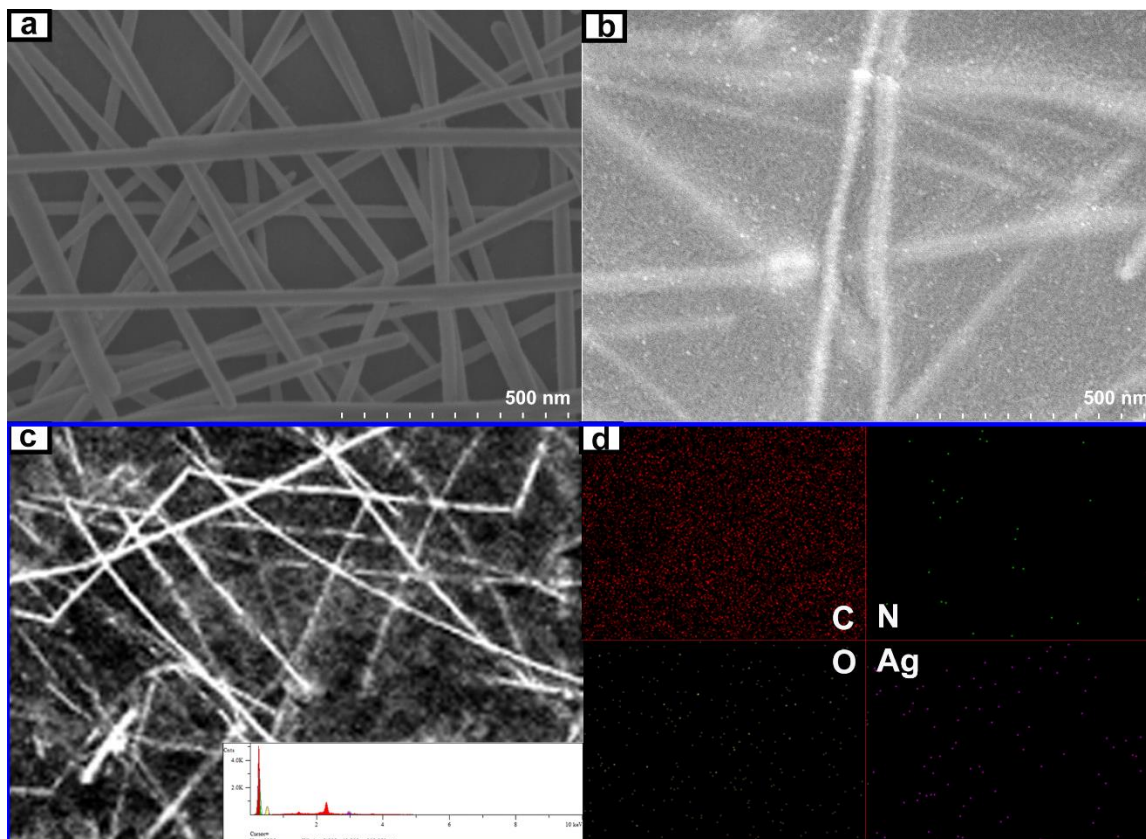

Fig. 1. (a) Morphology of AgNWs. (b) SEM images of AgNWs3/CE1@ACNC films; (c, d) The element map image of AgNWs3/CE1@ACNC films and the target element content of C, N, O, and Ag

Figure 1(b) shows the SEM image of an AgNWs3/CE1@ACNC composite film. The AgNWs network was evenly distributed on the ACNC surface, without fractures, collapse, or other defects. The ACNC substrate also remained smooth, without cracks, which indicates the compatibility between the two. In addition, the AgNWs made full

contact with each other, which helps to enhance their electrical conductivity and reduce the change in resistance. Figure 2(d) shows the XRD patterns of the ACNC, AgNWs, and AgNWs3/CE@ACNC. The peaks of ACNC appear at $2\theta = 20.6°$ and $22.3°$, corresponding to the (110) and (200) crystal planes (Jiang *et al*. 2019), respectively, indicating that it was mainly composed of cellulose type II crystal structure. With the addition of AgNWs, a diffraction peak appeared for AgNWs3/CE@ACNC at $2\theta = 38.28°$, and the other regions were consistent with ACNC, indicating that the materials were mixed well and remained stable during processing, including their crystal phases.
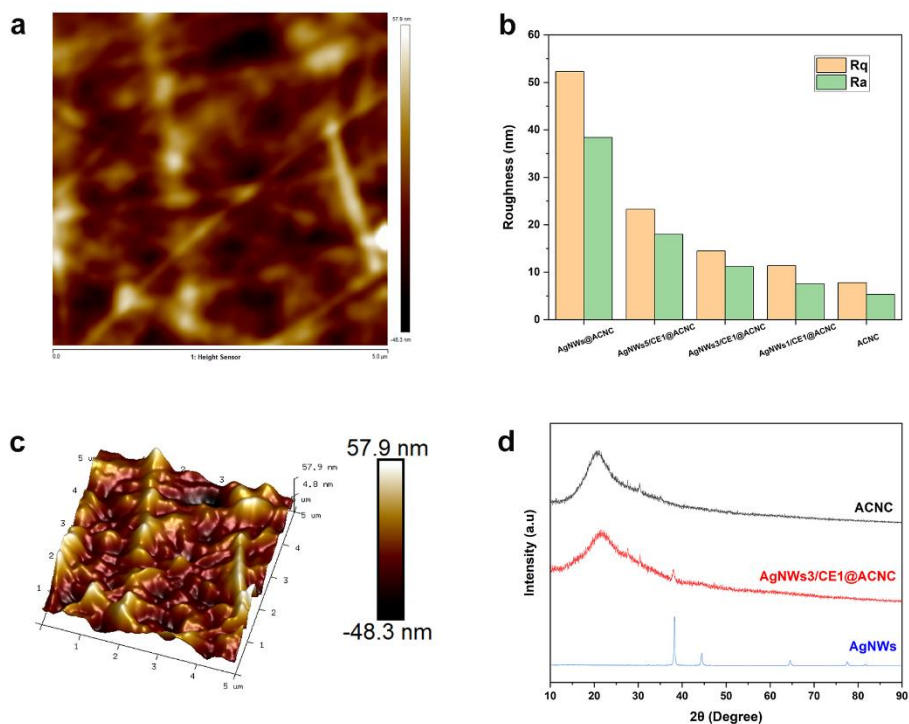

Fig. 2. AFM images of AgNWs3/CE@ACNC films (a, c); (b) R_a and R_q values for all films; (d) XRD patterns for all films

A representative AFM image of the AgNWs3/CE@ACNC composites is shown in Fig. 2(a). The corresponding root-mean-square roughness (R_q) and average roughness (R_a) of the AgNWs and AgNWs/ACNC films are shown in Fig. 3(b). The average roughness parameter R_a of common ACNC was 5.31 nm. This was lower than that of previous studies (Mohamed *et al*. 2015), likely because a higher polymer concentration generally increases the surface roughness (Wang *et al*. 2021). The R_a of the AgNWs/ACNC membrane composite was 38.2 nm, which was much higher than that of the ACNC membrane alone. This is attributed to the accumulation of AgNWs, forming undulations. The addition of cellulose significantly reduced the surface roughness compared with AgNWs/ACNC ($R_a = 38.4$ nm). At different AgNWs and cellulose content ratios, the roughness of FTEs films was significantly different. When the cellulose content was low, more AgNWs were exposed, especially the intersections of AgNWs, and the network structure exhibited higher roughness. In contrast, when the cellulose content was increased, more cellulose filled the gaps in the AgNWs network, forming a flatter film.

The results show that the method produced a uniform conductive network. The AgNWs were uniformly distributed with random orientation in all directions, and the

AgNWs network was partially or completely embedded in the regenerated cellulose membrane. The formation process is inferred as follows. The stability of this self-assembled structure is attributed to the hydrogen bonds between cellulose molecules, which are stronger than common van der Waals forces. The self-assembly process involves two main steps. The first step is the immersion and precipitation phase transition, in which the ionic liquid diffuses in water and the cellulose molecular chains wrapped around the surface of the AgNWs form hydrogen bonds with the hydroxy-rich ACNC film on the surface. Thus, the AgNWs are firmly fixed to the ACNC surface. In the second step, the subsequent drying process, the water-loss, and shrinkage between the cellulose molecular chains induce bending at the AgNWs contact sites, the physical contact is enhanced, and contact resistance is reduced, further strengthening the mechanical stability of the AgNWs conductive network.
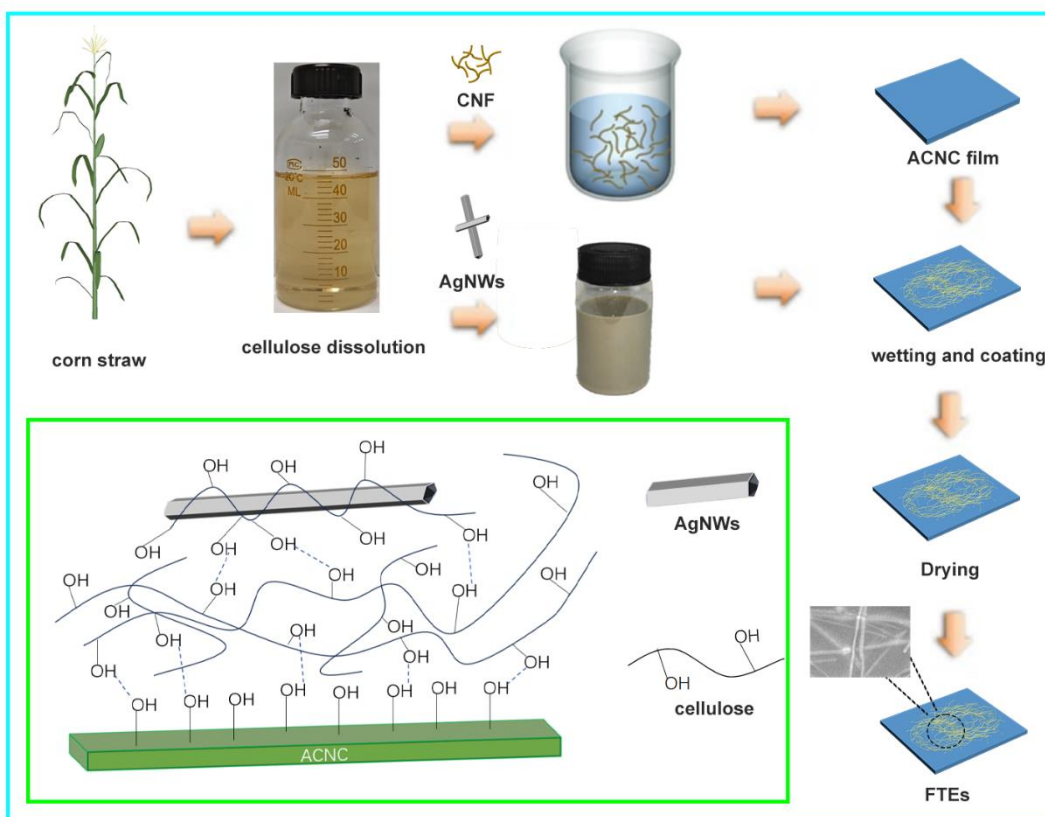
Fig. 3. Process diagram of cellulose-based FTEs preparation

Performance of the FTEs

For practical application in portable electronics, long-term flexibility and durability are required (Miao and Fan 2023). As shown in Fig. 4(a, b), tensile tests were conducted on all samples. With the increase in the AgNWs to cellulose ratio, the tensile strengths of the composite films gradually decreased, indicating that the mechanical strength of the composite film was supported by the cellulose network, which provided enhanced contact and stress transfer. Conversely, the increase in AgNWs in the composite film reduced the number of hydrogen bonds between cellulose molecules. Nonetheless, all composite films exhibited considerable mechanical strength (above 60 MPa). The tensile strength, particularly at the point of breakage, appears relatively constant across the samples, as indicated by the similar heights of the stress-strain curves in Fig (4a). What notably

changed was the elongation at break, with higher silver content samples demonstrating less elongation. This suggests that while the tensile strength remained consistent, the material's ductility, or ability to withstand deformation, was affected by the silver content. As shown in Fig. 4(b), AgNWs3/CE@ACNC films were able to withstand a 100 g load, withstand large deformation, and maintain their optical performance.
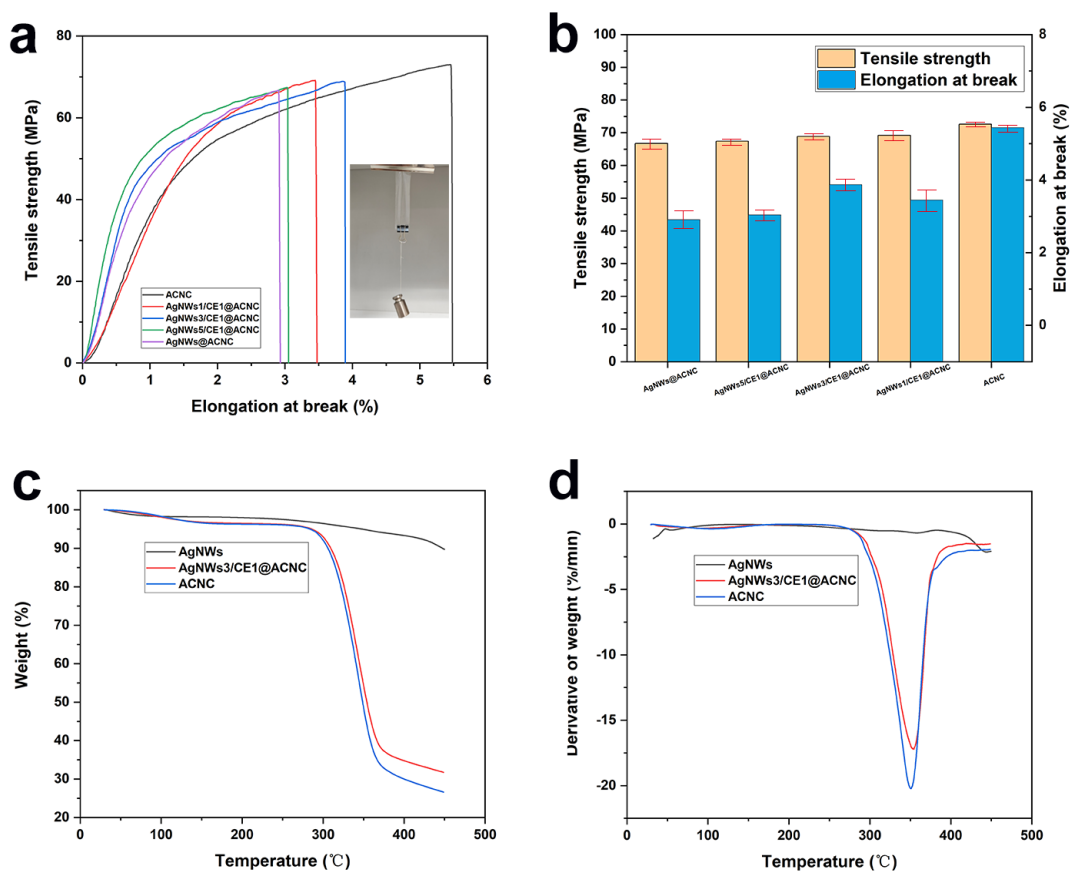

Fig. 4. (a, b) Tensile properties of all films. (c) TGA thermograms and (d) DTG curves of the AgNWs, ACNC, and AgNWs3\CE1@ACNC samples

The thermograms from thermogravimetric analysis (TGA) and derivative thermogravimetric (DTG) curves are shown in Figs. 4(c) and (d), respectively. AgNWs are relatively stable in nitrogen with no significant mass loss. Thus, the early mass loss observed in the AgNWs curves is attributed to small amounts of volatile GL and water molecules. The apparent drop after 300 °C is ascribed to the degradation and volatilization of organic functional groups in the PVP molecules on the surface of AgNWs. This is consistent with the analysis of N by SEM-EDS. In addition, ACNC and AgNWs3\CE1@ACNC exhibit a loss between room temperature and 120 °C. This is partially ascribed to water molecules present in thin films because of chemisorption and intermolecular hydrogen bonds. The main decomposition of both films occurs between 260 to 400 °C, indicating the decomposition of cellulose, nanocellulose, and PVP, which is consistent with observations in the literature (Du *et al*. 2006; D'Acierno *et al*. 2023). From the DTG curves, with the addition of AgNWs, the temperature corresponding to the maximum decomposition rate increases. These results indicate that the presence of AgNWs slightly improves the thermal stability of the composite film.
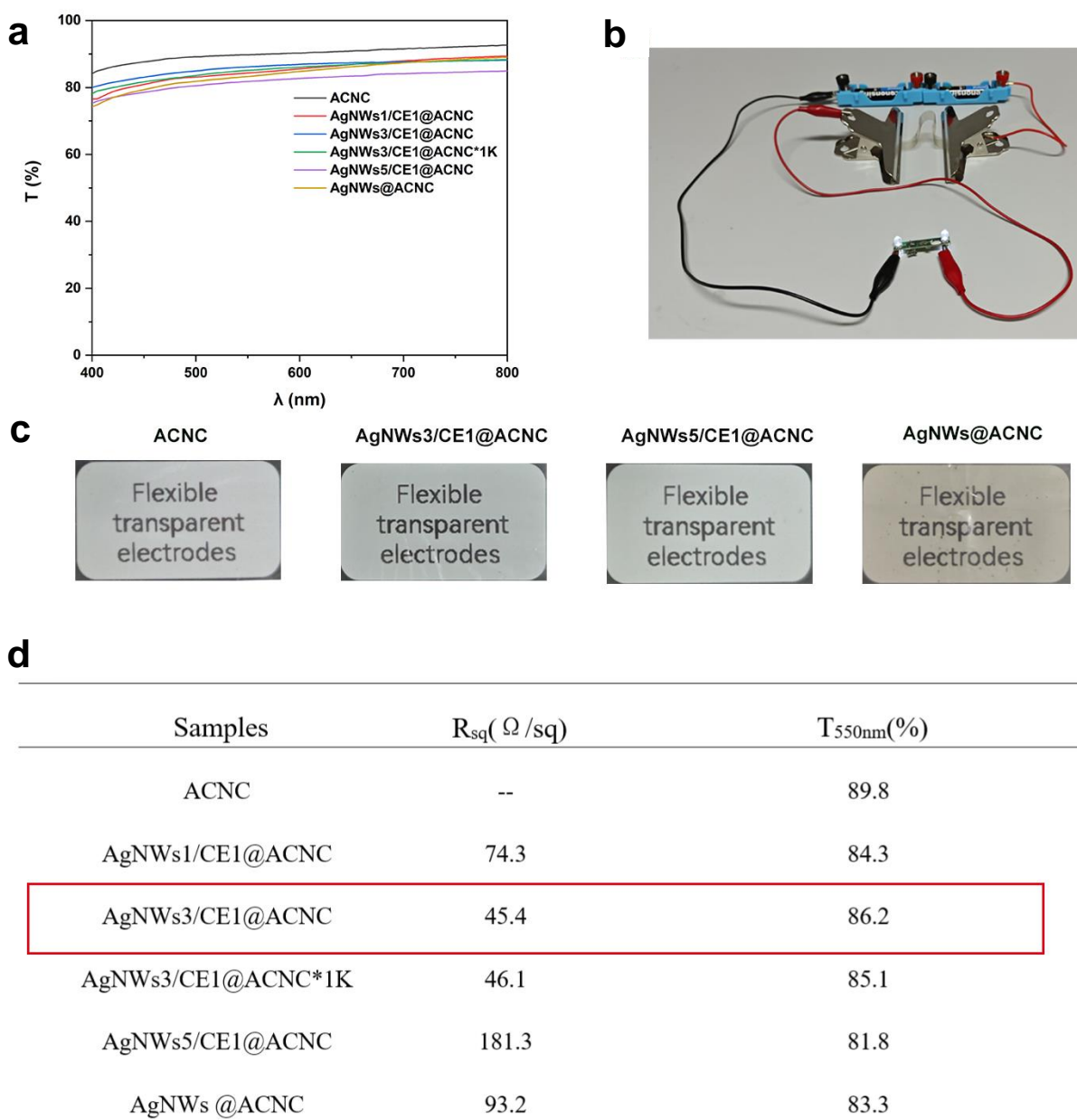
Fig. 5. (a) UV-Vis spectra of all films. Photos of the LED in series with AgNWs3\CE1@ACNC films. (c) Photos of the text covered by films. (d) Table of T_{550nm} and R_{sq} for all samples

Samples	R_{sq} (Ω /sq)	T_{550nm}(%)
ACNC	--	89.8
AgNWs1/CE1@ACNC	74.3	84.3
AgNWs3/CE1@ACNC	45.4	86.2
AgNWs3/CE1@ACNC*1K	46.1	85.1
AgNWs5/CE1@ACNC	181.3	81.8
AgNWs @ACNC	93.2	83.3

Photoelectric performance is an important aspect of FTEs for application in optoelectronic devices. As shown in Fig. 5(d), digital photos of the ACNC, AgNWs@ACNC, AgNWs3/CE1@ACNC, and AgNWs5/CE1@ACNC films on top of text are used to visualize and compare the films' optical transparency. The background text can be seen, confirming the high light transmission rate of the composite films. This is ascribed to the dense microstructure of the composite films, as observed in the SEM images, which greatly reduces the refraction and scattering caused by voids. Figure 5(c) shows the LED lamp under the applied voltage of 3 V. The observed color change in the film material with varying cellulose amounts, as shown in Fig. 5c, is due to factors such as altered light scattering and absorption, changes in the arrangement of cellulose molecules, chemical interactions within the film, and shifts in the refractive index. These changes in

the film's physical and chemical properties with different cellulose concentrations directly affect its optical characteristics, leading to visible color variations. The film composed of AgNWs3/CE1@ACNC, in its bent state, is used as the wire in series, and two LEDs are illuminated, which visually reveals the film's conductivity. Further evaluation was done on the transmittance (400 to 800 nm) and sheet resistance of the composite film in the visible light range. To better showcase the work, additional comparative data are provided in the supplementary information. (Table. S1)

Figure 5(a) shows the transmittance of composite films with different AgNWs loading, using the original ACNC as the control sample. By adjusting the ratio of cellulose and AgNWs, it was found that when the mass ratio of cellulose and AgNWs was 3:1, there was a higher transmittance. When the content of cellulose was low, the surface roughness of FTEs was large, which affects the transmittance. However, when the content of cellulose was too high, the AgNWs network tended to be loose in the direction perpendicular to the surface, resulting in a more complex scattering path. This is also consistent with the sheet resistance. When the mass ratio of AgNWs to cellulose is 1:1, the conductivity is significantly reduced owing to the increase in tunneling resistance (Zare and Rhee 2020).

In addition, optical stability is essential to extend the lifetime of flexible optoelectronic devices. Therefore, the change in the light transmittance of the AgNWs3/CE1@ACNC films was evaluated after performing the bending tests. As shown in Fig. 6(a), the light transmittance slightly decreased for AgNWs3/CE1@ACNC after bending 1000 times, which may be caused by the amplification of small defects in the substrate, but this result still indicates that the FTEs had relatively long-term stability.

At the same time, whether it is a flexible electric heater, a wearable device, or a component in a foldable display, its resistance change amplitude and durability in the bent state are important to consider (Zhang *et al*. 2021). These factors are related to the relative stability of the conductive AgNWs network and the stability of the connections between the conductive network and the substrate (Liu *et al*. 2021). Therefore, the flexural properties of the prepared composite films were analyzed. As shown in Figs. 6(b) and (c), the resistance changes during the folding and bending tests were analyzed. Whether the number of folds was increased, or the film was bent over a distance of 5 to 2 cm, the resistance change was on the order of 3%. After repeating the bending test 1000 times, the relative increase in resistance was also negligible. This is because of the interfacial compatibility between AgNWs and cellulose, as well as the stable hydrogen bonding between cellulose and ACNC, which reduces stress during deformation. Supported by the hydrogen bonding network of cellulose, the displacement of AgNWs is limited, and the conductive network structure is protected, thus achieving strong bending durability. These results suggest that the embedded AgNWs network maintains adhesion during bending, which means that additional measures to increase adhesion are unnecessary.

Additionally, the stability of AgNWs3/CE1@ACNC was tested after exposure to air. Under the average RH of 40% and an average temperature of 30 °C, the resistance of AgNWs3/CE1@ACNC films increased by only 2.5% after 16 days of exposure to air. To obtain more objective data, the oxygen permeability of the AgNWs3/CE1@ACNC membrane was tested, and it was found that the oxygen inhibition performance of FTEs was 0.000053 mL μm m^{-2} day^{-1} kPa^{-1}, which is higher than that of common petrochemical products on the market (Xia *et al*. 2018). This is due to the presence of nanofillers, specifically cellulose nanofibers and AgNWs, which make the membrane denser while also making the oxygen travel path narrower and longer. Owing to their excellent electromechanical stability and high chemical stability, FTEs embedded in AgNWs have great potential in many deformable optoelectronic devices.

Because cellulose has beneficial environmental characteristics, such as renewability and degradability, a simple biodegradation test was conducted on the prepared films in farmland soil. There was a reduction in the intact fragments of pure ACNC and composite membranes after 32 and 50 days of burial, respectively. Figure S2 shows the change in weight loss degradation of cellulose film in natural farmland soil over time. This is a type of biodegradation caused by soil microbes, which involves random breaking of cellulose macromolecular bonds during biodegradation (Tong *et al*. 2020). The presence of AgNWs delayed the process to a certain extent but still completed the natural degradation process, which proved the environmental protection of cellulose-based FTEs.
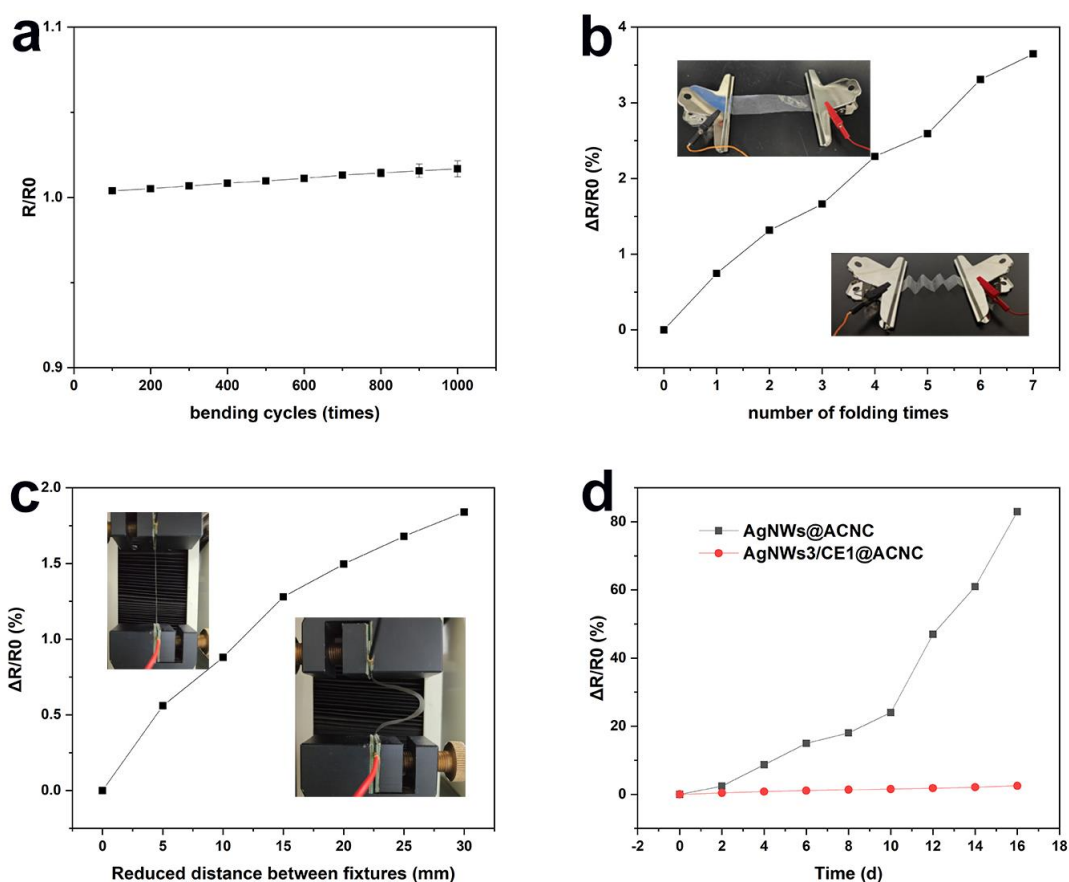

Fig. 6. Changes in sheet resistance ($\Delta R/R_0$) during the bending cycles (a), folding test, (b) and bending deformation (c) of AgNWs3/CE1@ACNC films. (d) Long-term testing of AgNWs3 @ACNC films and AgNWs3/CE1@ACNC films

CONCLUSIONS

1. A one-step coating formulation method was developed to produce flexible transparent electrodes (FTEs) with high flexibility and stability. The embedded cellulose-based FTEs were fabricated by dispersing silver nanowires (AgNWs) in cellulose solution and adhering AgNWs to the surface of the all-cellulose nanocomposite (ACNC) membrane by scraping and self-assembly. The cellulose is the mechanical support and protective layer, and the embedded AgNWs constitute the conductive network embedded in the surface layer.

2. The FTEs exhibited useful mechanical properties. Their thin layer resistance was 45.4 Ω/sq, and the light transmittance was 86.2 %. The FTEs maintained their conductivity under various deformation conditions, even after 1000 bending cycles. In addition, the FTEs exhibited biodegradable and environmentally friendly characteristics.

ACKNOWLEDGEMENTS

REFERENCES

Akter, T., and Kim, W. S. (2012). "Reversibly stretchable transparent conductive coatings of spray-deposited silver nanowires," *ACS Applied Materials & Interfaces* 4(4), 1855-1859. DOI: 10.1021/am300058j

Ashok Kumar, S. S., Bashir, S., Ramesh, K., and Ramesh, S. (2022). "A review on graphene and its derivatives as the forerunner of the two-dimensional material family for the future," *Journal of Materials Science* 57(26), 12236-12278. DOI: 10.1007/s10853-022-07346-x

Aziz, T., Haq, F., Farid, A., Kiran, M., Faisal, S., Ullah, A., Ullah, N., Bokhari, A., Mubashir, M., Chuah, L. F., and Show, P. L. (2023). "Challenges associated with cellulose composite material: Facet engineering and prospective," *Environmental Research* 2023, article 115429. DOI: 10.1016/j.envres.2023.115429

Calvino, C., Macke, N., Kato, R., and Rowan, S. J. (2020). "Development, processing and applications of bio-sourced cellulose nanocrystal composites," *Progress in Polymer Science* 103, article 101221. DOI: 10.1016/j.progpolymsci.2020.101221

D'Acierno, F., Michal, C. A., and MacLachlan, M. J. (2023). "Thermal stability of cellulose nanomaterials," *Chemical Reviews* 123(11), 7295-7325. DOI: 10.1021/acs.chemrev.2c00816

Du, Y. K., Yang, P., Mou, Z. G., Hua, N. P., and Jiang, L. (2006). "Thermal decomposition behaviors of PVP coated on platinum nanoparticles," *Journal of Applied Polymer Science* 99 (1), 23-26. DOI: 10.1002/app.21886

Fan, Q., Miao, J., Liu, X., Zuo, X., Zhang, W., Tian, M., Zhu, S., Qu, L., and Zhang, X. (2022). "Biomimetic hierarchically silver nanowire interwoven MXene mesh for flexible transparent electrodes and invisible camouflage electronics," *Nano Letters* 22(2), 740-750. DOI: 10.1021/acs.nanolett.1c04185

Fan, X. (2021). "Doping and design of flexible transparent electrodes for high-performance flexible organic solar cells: recent advances and perspectives," *Advanced Functional Materials* 31(8), article 2009399. DOI: 10.1002/adfm.202102717

Gill, M. K., Kocher, G. S., and Panesar, A. S. (2021). "Optimization of acid-mediated delignification of corn stover, an agriculture residue carbohydrate polymer for improved ethanol production," *Carbohydrate Polymer Technologies and Applications* 2, article 100029. DOI: 10.1016/j.carpta.2020.100029

Gorji, M., Mazinani, S., Faramarzi, A.-R., Ghadimi, S., Kalaee, M., Sadeghianmaryan, A., and Wilson, L. D. (2021). "Coating cellulosic material with Ag nanowires to fabricate wearable IR-reflective device for personal thermal management: The role of coating method and loading level," *Molecules* 26 (12), article 3570. DOI: 10.3390/molecules26123570

Guo, Y., Cai, L., Guo, G., Xie, H., Zhang, L., Jin, L., Liang, S., Hu, L., Xu, Q., and Zheng, Q. (2021). "Cellulose membranes from cellulose CO_2-based reversible ionic liquid solutions," *ACS Sustainable Chemistry & Engineering* 9 (35), 11847-11854. DOI: 10.1021/acssuschemeng.1c03609

Hamd, W., Daher, E. A., Tofa, T. S., and Dutta, J. (2022). "Recent advances in photocatalytic removal of microplastics: Mechanisms, kinetic degradation, and reactor design," *Frontiers in Marine Science* 9, article 885614. DOI: 10.3389/fmars.2022.885614

Hu, X., Li, X., Li, G., Ji, T., Ai, F., Wu, J., Ha, E., and Hu, J. (2021). "Recent progress of methods to enhance photovoltaic effect for self-powered heterojunction photodetectors and their applications in inorganic low-dimensional structures," *Advanced Functional Materials* 31(24), article 2011284. DOI: 10.1002/adfm.202011284

Janaswamy, S., Yadav, M. P., Hoque, M., Bhattarai, S., and Ahmed, S. (2022). "Cellulosic fraction from agricultural biomass as a viable alternative for plastics and plastic products," *Industrial Crops and Products* 179, article 114692. DOI: 10.1016/j.indcrop.2022.114692

Jiang, Z., Tang, L., Gao, X., Zhang, W., Ma, J., and Zhang, L. (2019). "Solvent regulation approach for preparing cellulose-nanocrystal-reinforced regenerated cellulose fibers and their properties," *ACS OMEGA* 4 (1), 2001-2008. DOI: 10.1021/acsomega.8b03601

Kumar, A. K., wan Bae, C., Piao, L., and Kim, S.-H. (2013). "Silver nanowire based flexible electrodes with improved properties: High conductivity, transparency, adhesion and low haze," *Materials Research Bulletin* 48(8), 2944-2949. DOI: 10.1016/j.materresbull.2013.04.035

Li, X., Yu, S., Zhao, L., Wu, M., and Dong, H. (2020). "Hybrid PEDOT: PSS to obtain high-performance AgNW-based flexible transparent electrodes for transparent heaters," *Journal of Materials Science: Materials in Electronics* 31, 8106-8115. DOI: 10.1007/s10854-020-03351-5

Li, Z., Zhong, L., Zhang, T., Qiu, F., Yue, X., and Yang, D. (2019). "Sustainable, flexible, and superhydrophobic functionalized cellulose aerogel for selective and versatile oil/water separation," *ACS Sustainable Chemistry & Engineering* 7(11), 9984-9994. DOI: 10.1021/acssuschemeng.9b01122

bioresources.cnr.ncsu.edu

Liu, X., Miao, J., Fan, Q., Zhang, W., Zuo, X., Tian, M., Zhu, S., Zhang, X., and Qu, L. (2021). "Smart textile based on 3D stretchable silver nanowires/MXene conductive networks for personal healthcare and thermal management," *ACS Applied Materials & Interfaces* 13(47), 56607-56619. DOI: 10.1021/acsami.1c18828

Ma, C., Liu, Y.-F., Bi, Y.-G., Zhang, X.-L., Yin, D., Feng, J., and Sun, H.-B. (2021). "Recent progress in post treatment of silver nanowire electrodes for optoelectronic device applications," *Nanoscale* 13 (29), 12423-12437. DOI: 10.1039/d1nr02917g

Miao, J., and Fan, T. (2023). "Flexible and stretchable transparent conductive graphene-based electrodes for emerging wearable electronics," *Carbon* 202, 495-527. DOI: 10.1016/j.carbon.2022.11.018

Min, S.-H., Kim, C. K., Lee, H.-N., and Moon, D.-G. (2012). "An OLED using cellulose paper as a flexible substrate," *Molecular Crystals and Liquid Crystals* 563(1), 159-165. DOI: 10.1080/15421406.2012.689153

Mohamed, M. A., Salleh, W., Jaafar, J., Ismail, A., Abd. Mutalib, M., and Jamil, S. M. (2015). "Feasibility of recycled newspaper as cellulose source for regenerated cellulose membrane fabrication," *Journal of Applied Polymer Science* 132(43). DOI: 10.1002/app.42684

Qian, C., Xiao, T., Chen, Y., Wang, N., Li, B., and Gao, Y. (2022). "3D printed reduced graphene oxide/elastomer resin composite with structural modulated sensitivity for flexible strain sensor," *Advanced Engineering Materials* 24(4), article 2101068. DOI: 10.1002/adem.202101068

Qin, Y., Yao, L., Zhang, F., Li, R., Chen, Y., Chen, Y., Cheng, T., Lai, W., Mi, B., Zhang, X., and Huang, W. (2022). "Highly stable silver nanowires/biomaterial transparent electrodes for flexible electronics," *ACS Applied Materials & Interfaces* 14(33), 38021-38030. DOI: 10.1021/acsami.2c0915338021

Rieland, J. M., and Love, B. J. (2020). "Ionic liquids: A milestone on the pathway to greener recycling of cellulose from biomass," *Resources, Conservation and Recycling* 155, article 104678. DOI: 10.1016/j.resconrec.2019.104678

Sang, J., Zhang, J., Feng, H., Sun, J., Shang, J., Zhang, Y., Zhao, S., Neyts, K., and Chigrinov, V. (2022). "Flexible and transferable silver nanowire liquid crystal polymer film obtained via photo-alignment programming," *Advanced Optical Materials* 10(16), article 2200950. DOI: 10.1002/adom.202200950

Shen, X., Zheng, Q., and Kim, J.-K. (2021). "Rational design of two-dimensional nanofillers for polymer nanocomposites toward multifunctional applications," *Progress in Materials Science* 115, article 100708. DOI: 10.1016/j.pmatsci.2020.100708

Sun, H., Lu, Y., Chen, Y., Yue, Y., Jiang, S., Xu, X., Mei, C., Xiao, H., and Han, J. (2022a). "Flexible environment-tolerant electroluminescent devices based on nanocellulose-mediated transparent electrodes," *Carbohydrate Polymers* 296, 119891. DOI: 10.1016/j.carbpol.2022.119891

Sun, J., Ahn, H., Kang, S., Ko, S.-B., Song, D., Um, H. A., Kim, S., Lee, Y., Jeon, P., Hwang, S.-H., You, Y., Chu, C., and Kim, S. (2022b). "Exceptionally stable blue phosphorescent organic light-emitting diodes," *Nature Photonics* 16(3), 212-218. DOI: 10.1038/s41566-022-00958-4

Tan, K. Y., Hoy, Z. X., Show, P. L., Huang, N. M., Lim, H. N., and Foo, C. Y. (2021). "Single droplet 3D printing of electrically conductive resin using high aspect ratio silver nanowires," *Additive Manufacturing* 48, article 102473. DOI: 10.1016/j.addma.2021.102473

Tong, R., Chen, G., Tian, J., and He, M. (2020). "Highly transparent, weakly hydrophilic and biodegradable cellulose film for flexible electroluminescent devices," *Carbohydrate Polymers* 227, article 115366. DOI: 10.1016/j.carbpol.2019.115366

Valderrama, J., and Robles, P. (2007). "Critical properties, normal boiling temperatures, and acentric factors of fifty ionic liquids," *Industrial & Engineering Chemistry Research* 46 (4), 1338-1344. DOI: 10.1021/ie070413+

Wang, H., Wang, Y., and Chen, X. (2019). "Synthesis of uniform silver nanowires from AgCl seeds for transparent conductive films via spin-coating at variable spin-speed," *Colloids and Surfaces A: Physicochemical and Engineering Aspects* 565, 154-161. DOI: 10.1016/j.colsurfa.2018.11.050

Wang, Y., Li, Q., Miao, W., Lu, P., You, C., and Wang, Z. (2021). "Hydrophilic PVDF membrane with versatile surface functions fabricated via cellulose molecular coating," *Journal of Membrane Science* 640, article 119817. DOI: 10.1016/j.memsci.2021.119817

Wu, X., Wang, S., Luo, Z., Lu, J., Lin, K., Xie, H., Wang, Y., and Li, J.-Z. (2021). "Inkjet printing of flexible transparent conductive films with silver nanowires ink," *Nanomaterials* 11(6), 1571. DOI: 10.3390/nano11061571

Xia, J., Zhang, Z., Liu, W., Li, V. C., Cao, Y., Zhang, W., and Deng, Y. (2018). "Highly transparent 100% cellulose nanofibril films with extremely high oxygen barriers in high relative humidity," *Cellulose* 25, 4057-4066. DOI: 10.1007/s10570-018-1843-y

Xie, Y., Gao, H., Zhang, P., Qin, C., Nie, Y., and Liu, X. (2022). "Preparation of degradable wood cellulose films using ionic liquids," *ACS Applied Nano Materials* 4 (5), 3598-3607. DOI: 10.1021/acsapm.2c00167

Zare, Y., and Rhee, K. Y. (2020). "Significances of interphase conductivity and tunneling resistance on the conductivity of carbon nanotubes nanocomposites," *Polymer Composites* 41 (2), 748-756. DOI: 10.1002/pc.25405

Zhang, H., Dou, C., Pal, L., and Hubbe, M. A. (2019). "Review of electrically conductive composites and films containing cellulosic fibers or nanocellulose," *BioResources* 14(3), 7494-7542. DOI: 10.15376/biores.14.3.7494-7542

Zhang, L., Jiang, Z., Yang, S., Zeng, Z., Zhang, W., and Zhang, L. (2020). "Different rheological behaviours of cellulose/tetrabutylammonium acetate/dimethyl sulfoxide/water mixtures," *Cellulose* 27, 7967-7978. DOI: 10.1007/s10570-020-03363-8

Zhang, T., Yang, P., Li, Y., Cao, Y., Zhou, Y., Chen, M., Zhu, Z., Chen, W., and Zhou, X. (2019). "Flexible transparent sliced veneer for alternating current electroluminescent devices," *ACS Sustainable Chemistry & Engineering* 7(13), 11464-11473. DOI: 10.1021/acssuschemeng.9b01129

Zhang, Y., Guo, X., Wang, W., Chen, L., Liu, L., Liu, H., and He, Y. (2020). "Highly sensitive, low hysteretic and flexible strain sensor based on ecoflex-AgNWs-MWCNTs flexible composite materials," *IEEE Sensors Journal* 20 (23), 14118-14125. DOI: 10.1109/JSEN.2020.3008159

Zhang, Y., Ren, H., Chen, H., Chen, Q., Jin, L., Peng, W., Xin, S., and Bai, Y. (2021). "Cotton fabrics decorated with conductive graphene nanosheet inks for flexible wearable heaters and strain sensors," *ACS Applied Nano Materials* 4 (9), 9709-9720. DOI: 10.1021/acsanm.1c02076

Zhao, G., Lyu, X., Lee, J., Cui, X., and Chen, W.-N. (2019). "Biodegradable and transparent cellulose film prepared eco-friendly from durian rind for packaging application," *Food Packaging and Shelf Life* 21, article 100345. DOI: 10.1016/j.fpsl.2019.100345

Zhu, H., Shin, E. S., Liu, A., Ji, D., Xu, Y., and Noh, Y. Y. (2020). "Printable semiconductors for backplane TFTs of flexible OLED displays," *Advanced Functional Materials* 30 (20), 1904588. DOI: 10.1002/adfm.201904588

APPENDIX
Supplementary Information

(https://watch.wave.video/JGR7ahhHbjfG3Rbu)
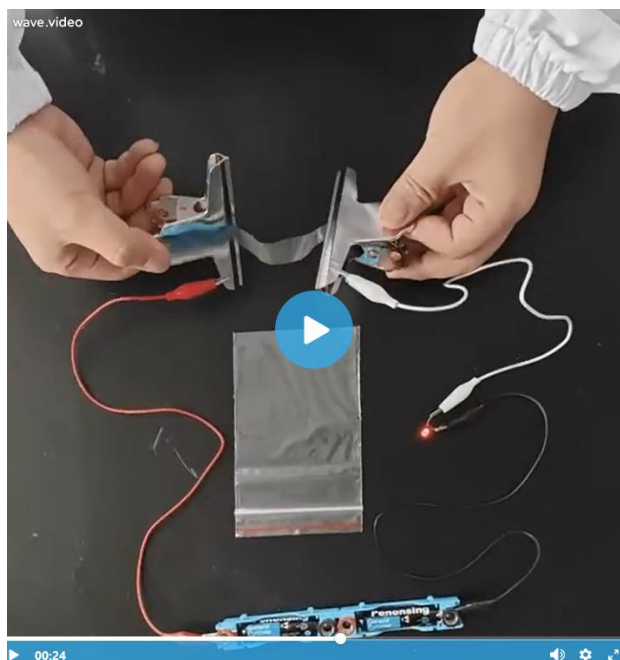
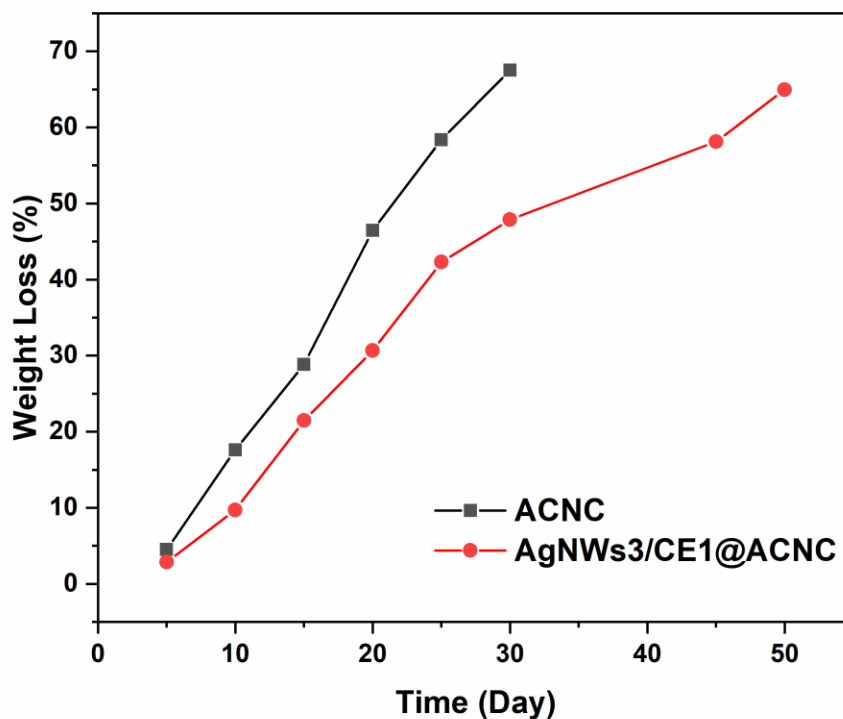**Fig. S1.** Videos of the LED in series with AgNWs3\CE1@ACNC films

Fig. S2. The biodegradability of ACNC and AgNWs3\CE1@ACNC films in soil

Table S1. Comparison of This Work to Recent Work on High-performance Transparent Electrodes

Substrate	Conductive Materials	Transparency (%)	Wave-length	Sheet Resistance	Reference
ACNC	AgNWs/Cellulose	86.2	550 mm	45.35	This work
PET	AgNWs/HEC	86.7	550 mm	68	Ao *et al.* (2023)
PET	Polyurethane/AgNWs	73	550 mm	143	Judic et al. (2023)
NFC-HS	AgNWs	83.3	600 mm	30	Yu *et al.* (2021)
RC	PEDOT:PSS/AgNW	73.8	550 mm	11.2	Kwon *et al.* (2024)
CNF	RGO	76	550 mm	2.5k	Gao *et al.* (2013)
TEMPO-CNF	AgNW	82	550 mm	54	Kim *et al.* (2018)
BC	AgNWs	<80	550 mm	7.46	Lv *et al.* (2018)
PET	AgNWs/PVA	77	550 mm	15	Lu *et al.* (2019)

References for Table S1

Ao, H., Feng, J., Cao, P., Yang, T., Shang, T., and Xing, B. (2023)." Synthesis of Ag nanowires with an aspect ratio higher than 2000 for the fabrication of transparent conductive film," *Journal of Materials Science: Materials in Electronics* 34(33), 2183. DOI:10.1007/s10854-023-11579-0

Gao, K., Shao, Z., Wu, X., Wang, X., Li, J., Zhang, Y., Wang, W., and Wang, F. (2013). "Cellulose nanofibers/reduced graphene oxide flexible transparent conductive paper," *Carbohydrate Polymers* 97(1), 243-251. DOI:10.1016/j.carbpol.2013.03.067

Judic, M., Lonjon, A., Dantras, E., and Lacabanne, C. (2023)." One-step elaboration of flexible transparent conductive electrodes from silver nanowires/polymer nanocomposites,"*Journal of Applied Polymer Science* e55117. DOI:10.1002/app.55117

Kim, D., Y. Ko, G. Kwon, U.-J. Kim and J. You. (2018)." Micropatterning Silver Nanowire Networks on Cellulose Nanopaper for Transparent Paper Electronics," *ACS Applied Materials & Interfaces* 10(44), 38517-38525. DOI:10.1021/acsami.8b15230

Kwon, G., Ko, Y., Lee, K., Jeon, Y., Lee, S., Lee, C., and You, J. (2024)." Flexible and transparent cellulose-based electrothermal composites for high-performance heaters,"*Cellulose* 31, 335-347. DOI:10.1007/s10570-023-05665-z

Lu, H., Luo, J., Liu, Y., Zhong, Y., Wang, J., and Zhang, Y. (2019)." Highly performance flexible polymer solar cells by flipping the bilayer film of Ag nanowires and polyvinyl alcohol on polyethylene terephthalate as transparent conductive electrodes," *IEEE Journal of Photovoltaics* 9(3), 710-714. DOI:10.1109/JPHOTOV.2019.2899469

Lv, P., Zhou, H., Zhao, M., Li, D., Lu, K., Wang, D., Huang, J., Cai, Y., Lucia, L. A., and Wei, Q. (2018)." Highly flexible, transparent, and conductive silver nanowire-attached bacterial cellulose conductors," *Cellulose* 25(6), 3189-3196. DOI:10.1007/s10570-018-1773-8

Yu, H., Tian, Y., Dirican, M., Fang, D., Yan, C., Xie, J., Jia, D., Liu, Y., Li, C., Cui, M., Liu, H., Chen, G., Zhang, X., and Tao, J. (2021)." Flexible, transparent and tough silver nanowire/nanocellulose electrodes for flexible touch screen panels," *Carbohydrate Polymers* 273, 118539. DOI:10.1016/j.carbpol.2021.118539

bioresources.cnr.ncsu.edu

NOTES:
For corn straw pulp:
α- Cellulose content --84%

Lignin content --2.34%
Cellulose content --89.62%
Hemicellulose content --8.04%
Degree of polymerization (viscosity-average molecular weight) --1700~1750